



HAL
open science

Application of gel polymer electrolytes based on ionic liquids in lithium-sulfur batteries

M. Baloch, A. Vizintin, R.K. Chellappan, J. Moskon, D. Shanmukaraj, Rémi Dedryvère, T. Rojo, R. Dominko

► To cite this version:

M. Baloch, A. Vizintin, R.K. Chellappan, J. Moskon, D. Shanmukaraj, et al.. Application of gel polymer electrolytes based on ionic liquids in lithium-sulfur batteries. *Journal of The Electrochemical Society*, 2016, 163 (10), pp.A2390. 10.1149/2.1151610jes . hal-01498742

HAL Id: hal-01498742

<https://hal.science/hal-01498742>

Submitted on 29 Mar 2024

HAL is a multi-disciplinary open access archive for the deposit and dissemination of scientific research documents, whether they are published or not. The documents may come from teaching and research institutions in France or abroad, or from public or private research centers.

L'archive ouverte pluridisciplinaire **HAL**, est destinée au dépôt et à la diffusion de documents scientifiques de niveau recherche, publiés ou non, émanant des établissements d'enseignement et de recherche français ou étrangers, des laboratoires publics ou privés.

1 **Application of Gel Polymer Electrolytes Based on Ionic Liquids in**
2 **Lithium-Sulfur Batteries**

3 Marya Baloch,^{a, b, =} Alen Vizintin,^{c, =} Rajesh Kumar Chellappan,^d Joze Moskon,^c Devaraj Shanmukaraj,^a
4 Rémi Dedryvère,^{d, e} Teofilo Rojo,^{a, b} and Robert Dominko^{c, e, *}

5
6 ^a CIC Energigune, Parque Tecnológico de Álava, CIC 01510 Miñano, Spain

7 ^b Departamento de Química Inorgánica, Universidad del País Vasco UPV/EHU, 48080 Bilbao, Spain

8 ^c National Institute of Chemistry, 1000 Ljubljana, Slovenia

9 ^d IPREM, CNRS, University Pau & Pays Adour, 64053 Pau cedex 9, France

10 ^e Alistore - European Research Institute, 80039 Amiens cedex, France

11

12

13

=These authors equally contributed to this work.

14

*E-mail: Robert.Dominko@ki.si

15

16

17 **Abstract**

18 In this study, a gel polymer electrolyte (GPE) based on polymer ionic liquid (PIL) is used in a
19 solvent-free and in a hybrid electrolyte configuration for Li-S batteries. Results obtained in
20 the solvent-free configuration show a high discharge capacity in the first cycle and excellent
21 coulombic efficiency during cycling. Capacity fading and polarization increase during cycling
22 are explained based on the XPS and EIS measurements. The results of the present study are
23 indicating that the increase of various internal resistance contributions and capacity fading are
24 related with an accumulation of polysulfides in the GPE-PIL layer or/and on the surface of the
25 lithium anode. Within a hybrid battery configuration, the thickness of the GPE-PIL layer is
26 thinner, and the volume where polysulfides can be trapped is smaller. Such a configuration
27 shows better cycling stability. The hybrid configuration outperforms cycling stability of the
28 conventional configuration with a liquid electrolyte. This is explained by increased internal
29 resistance in the conventional configuration while the polarization in the first 100 cycles is
30 constant in the hybrid configuration. Additionally, the hybrid configuration exhibits excellent
31 C-rate performance.

32

33 Manuscript submitted May 26, 2016; revised manuscript received August 3, 2016. Published
34 xx xx, xxxx.

35

36 1. Introduction

37 Lithium-sulfur (Li-S) batteries possess high theoretical specific capacity at potential of 2.15 V
38 and are expected to reach practical gravimetric energy density up to 600 Wh kg^{-1} .¹⁻⁴ Sulfur is
39 an abundant and easy element to handle. However, at room temperature is an insulator and
40 requires to be properly electrochemically wired.

41 Li-S battery working principles and the problems within system has been well-known for
42 decades.⁵⁻⁷ During discharge, two well defined plateaus at 2.4 V and 2.15 V, represent
43 equilibrium states between solid-state phase (either elemental sulfur or Li_2S) and polysulfides,
44 respectively.⁸ Recent research has been mainly focused on the development of suitable host
45 structures for sulfur *i.e.* porous structured carbons or oxide based materials.^{3,9-15} In addition,
46 attention has been drawn towards the development of new binders,^{16,17} separators,¹⁸⁻²⁰
47 electrolytes²¹⁻²³ and lithium protection.^{24,25}

48 Different types of electrolyte solvents (organic, aqueous and ionic liquids), salts, additives and
49 states (liquid, solid or polymer) has been proposed and tested in Li-S batteries. Most of the
50 work has been done with electrolytes based on ether solvents which are stable towards
51 polysulfides and possess high polysulfide solubility. Their major drawback is a severe shuttle
52 effect.²⁶ Polymer and solid-state electrolytes can suppress the shuttling effect, although the
53 rate capability is poor compared to liquid electrolytes.

54 Gel polymer electrolytes are the hybrid of conventional and solid polymer electrolytes with an
55 embedded liquid component, *i.e.* an electrolyte in a polymer matrix. Due to an immobilized
56 electrolyte, enhanced ionic conductivity is achieved, when compared to solid-state
57 electrolytes.²⁶ Moving from liquid to polymer electrolyte systems, safety of the battery system
58 enhances due to reduced probability for internal short-circuiting, absence of volatile reaction
59 products and no electrolyte leakage.²⁶⁻²⁹ Gel polymer electrolytes is an attractive choice for
60 Li-S batteries^{26,30-33} since it can simultaneously act as a binder and electrolyte due to the

61 presence of polymer material. Currently, polyvinylidene fluoride (PVdF)¹⁶ is the most
62 common used binder in Li-S batteries, processed by dissolving in *N*-methyl-2-pyrrolidone
63 (NMP). Generally electrode processing requires high drying temperatures under vacuum³⁴
64 that could lead to sulfur sublimation whereas, drying at lower temperatures leaves a
65 possibility of contamination with remaining NMP solvent.³⁴ In addition, the morphology of
66 hydrophobic polymers such as PVdF, blocks the pores³⁵ in the composite electrode, which
67 limits the electrolyte access and thereby affects ionic pathways. Recently the use of
68 alternative binders, such as polyvinyl pyrrolidone (PVP),³⁶ polytetrafluoroethylene (PTFE),³⁷
69 polyethylene oxide (PEO)³⁷ and water soluble binders such as carbonyl- β -cyclodextrin (C- β -
70 CD), etc.^{17,38,39} has been reported in Li-S batteries.

71 Herein, we present the application of a gel polymer electrolyte,⁴⁰ which can act as an
72 electrolyte and binder in Li-S battery. The GPE (poly(DDA)TFSI-PYR₁₄TFSI-LiTFSI) is
73 composed of 58 wt. % polymer ionic liquid: poly (diallyldimethylammonium)
74 bis(trifluoromethanesulfonyl)imide (poly (DDA)TFSI), and 1:9 mol ratio of ionic liquid: *N*-
75 butyl-*N*-methylpyrrolidinium bis(trifluoromethanesulfonyl)imide (PYR₁₄TFSI) with lithium
76 salt: Lithium bis(trifluoromethylsulphonyl)imide (LiTFSI) as shown in the Figure S1.

77 The gel polymer electrolyte, GPE-PIL, has been used as a self-standing membrane separator
78 in solvent-free battery configuration and as a binder in the composite cathode. Room
79 temperature cycling was obtained using a hybrid configuration of the cell containing a GPE-
80 PIL combined with liquid electrolyte leading to improved cycling properties compared to
81 conventional Li-S cells solely containing the liquid electrolyte. Due to the pronounced
82 binding properties of the GPE, no additional binder was required in the composite cathode.
83 This led to simplified electrode processing by replacement of NMP with acetonitrile or
84 acetone as a solvent for the composite slurry processing.

85

86 **2. Experimental**

87 Membrane preparation:

88 GPE membranes were prepared inside an argon-filled glove box. The GPE-PIL solution was
89 cast on the Mylar film support to form a homogeneous film, dried for over 24 h at room
90 temperature under argon atmosphere. The obtained film was peeled off from the support as a
91 self-standing membrane with thickness of ~200 μm (Figure S2).

92 Cathode composite preparation and cell assembly:

93 The gel polymer electrolyte was introduced in the composite cathode by two different
94 methods.

95 a) Impregnation of as-prepared electrode composites with GPE-PIL: Electrodes casted on
96 aluminum current collector were used with 50 wt. % sulfur loading in mesoporous carbon⁴¹
97 mixed with PVdF (Sigma-Aldrich, 99.98%) and carbon black (Printex XE2) in a mass ratio of
98 80:10:10 in NMP. The typical sulfur loading on the electrode was slightly above
99 1 mg per cm^2 . Electrodes were impregnated with the GPE-PIL solution and as a prepared
100 self-standing membrane (4.16 cm^2) was placed on top. The composite electrode was left to
101 dry slowly at room temperature (for at least 24 h). Both steps were carried out inside an
102 argon-filled glove box. The configuration of the solvent-free cell assembly is shown in Figure
103 S3. Briefly, lithium foil (Aldrich) was separated from the impregnated cathode by the GPE-
104 PIL membrane, and electrochemical performance of the obtained stack was measured in
105 pouch cells at 55 $^\circ\text{C}$ using C/40 rate in a 1.0–3.8 V voltage range. Galvanostatic
106 measurements were done using a Bio-Logic VMP3 galvanostat/potentiostat.

107 b) Mixing of sulfur/carbon composite with GPE-PIL. The sulfur/carbon composite was
108 prepared by using DMSO solvent technique. 30 wt. % of carbon black (Ketjan black
109 ECP600JD from AkzoNobel) and 70 wt. % of sulfur (Sigma-Aldrich, 99.98%) were
110 mixed in DMSO and stirred overnight at 155 $^\circ\text{C}$ in a closed vial. The obtained

111 mixture was centrifuged for 45 mins at 400 rpm, the acquired product was dried at
112 60 °C for 24 h under vacuum. This composite mixture (50 wt. %) was wet ball-milled
113 with 50 wt. % of GPE-PIL for 30 mins in acetonitrile. The slurry was casted on
114 carbon-coated aluminum current collector and dried overnight at 50 °C under
115 vacuum. Electrodes were punched out as spherical discs of 16 mm diameter. The
116 typical sulfur loading on the electrode was around 0.7 mg per cm⁻². Pouch cell-type
117 batteries were assembled in an argon-filled glove box. Conventional
118 cathode/electrolyte/anode battery configuration has been followed. GPE-PIL-C_{ECP600JD}-S
119 were used as cathode and lithium metal foil (Aldrich) as an anode separated by Celgard 2400
120 separator wetted with 1M LiTFSI in TEGDME:Diox (vol. 1:1) or 1M LiTFSI in DME:Diox
121 (vol. 1:1) electrolyte. The electrochemical performance was measured at room temperature
122 using C/20 rate in a 1.5–3 V voltage range using a Bio-Logic VMP3 galvanostat/potentiostat.
123 For comparative evaluation of the electrochemical properties with and without the use of
124 GPE-PIL as binders, conventional cathodes with PVdF binder were prepared by mixing
125 80 wt. % of C-S composite, 10 wt. % of ECP600JD carbon black and 10 wt. % of PVdF
126 in NMP. The slurry was wet ball-milled for 30 min in NMP and casted on carbon-
127 coated aluminum current collector. Electrodes were dried at 55 °C for 24 h prior to
128 use. Conditions for battery assembly and galvanostatic cycling tests of the PVdF-C_{ECP600JD}-S
129 cathodes were exactly the same as in the case of GPE-PIL-C_{ECP600JD}-S cathodes.

130 Impedance spectroscopy:

131 AC impedance responses were measured using Solartron SI 1260 impedance analyzer coupled
132 with PAR EG&G 283 potentiostat/galvanostat applying voltage-controlled sinusoidal signals
133 in the frequency range from 100 kHz to 1 mHz with an amplitude of 10 mV (rms).
134 Intermittent measurements were carried on the cell for every 2.5 hours during galvanostatic
135 cycling.

136 X-ray Photoelectron Spectroscopy (XPS):

137 XPS measurements were carried out with a Kratos Axis Ultra spectrometer with
138 monochromatic Al K α radiation ($h\nu = 1486.6$ eV). Battery opening was done in a controlled
139 argon atmosphere. The samples were transferred into vacuum through a glove box directly
140 connected to the XPS spectrometer without exposure to air or moisture. The binding energy
141 scale was calibrated using a C 1s hydrocarbon contamination peak at 285 eV. The electrodes
142 for the XPS analysis were not washed in any organic solvents before the XPS measurements.
143 Other experimental details has been reported elsewhere.⁴²

144 SEM analysis:

145 SEM images were measured with a field-emission scanning electron microscope (FE SEM)
146 Supra 35 VP (Zeiss, Germany).

147

148 **3. Results and discussion**

149

150 **3.1 Contributions of the GPE-PIL components to the internal resistance of the cell**

151 In order to get insight in the various contributions of different components and contacts in the
152 studied Li-S battery configurations we have performed an electrochemical impedance
153 spectroscopy (EIS) measurements. Due to the complexities of the system, we show in this
154 work only preliminary results, which will be discussed more in details in the future.

155

156 **a) Equivalent circuit of a conventional Li-S cell**

157 A proposed equivalent circuit of a conventional Li-S cell comprising a porous composite
158 cathode is presented in Figure 1. It is split to the corresponding contributions of the cathode,
159 anode and separator layer. The contribution of the electrolyte phase in the separator is
160 presented by parallel coupling of resistance $R_b(sep.)$ and capacitance C_ϵ which stands for the

161 capacitance associated with the dielectric relaxation in the electrolyte. Since the
162 corresponding time constant $R_b(sep.) \cdot C_\epsilon$ is typically in the order of 1 ns up to few 10 ns the
163 impedance contribution of the electrolyte in the separator for the practical frequency range of
164 EIS can usually be regarded as an Ohmic resistance $R_b(sep.)$. The same reasoning holds true
165 for the part of electrolyte that is present in the cathode pores – *i.e.* the parallel coupled pairs of
166 elements $r_{pore,i} || C_{e,i}$ can be regarded as pure Ohmic resistances $r_{pore,i}$.

167 The impedance contribution(s) of the Li-anode side vary during cycling (especially in the
168 initial cycles there is regularly observed a decrease in the anode impedance) similarly as
169 observed in Li-ion systems.^{43,44}

170 The contribution(s) of the porous cathode can be essentially presented by a modified type of
171 the transmission line model that was used for the interpretation of electro-chemical properties
172 of multi-particle Li-ion insertion cathodes.^{45,46} A Li-S cathode differs from a Li-ion cathode in
173 two major respects. First, the end members of the conversion reaction are solids with low
174 solubility while the intermediate polysulfides formed during the course of the reaction are
175 soluble in the ether-based electrolytes. Second, electrochemical redox reaction of soluble
176 sulfur species proceeds at the accessible surface of electronically conductive matrix while
177 chemical equilibrium tends to be established within the volume of electrolyte by means of
178 reaction between different sulfur species. As a consequence, the concentration gradients of
179 different sulfur species build up during the operation of the Li-S cell and simultaneously an
180 inevitable diffusion of those species is taking place. Although during operation of the Li-S
181 cell the situation in the electrolyte and at surface of conductive matrix is greatly complex
182 compared to the Li-ion cell. The impedance response of the Li-S cell in a quasi-equilibrium
183 state can be in a simplified manner treated similarly to a Li-ion cell with multi-particle
184 porous insertion cathode. When applying a small a.c. voltage signal during impedance
185 measurement of a quasi-equilibrated Li-S cell the variations of concentrations of the present

186 sulfur species are small and for the present purpose we neglect the effect of these
187 concentration variations on the ion transport in the electrolyte. The cathode composite is
188 assumed to be homogeneous – thus it can be split in the serially connected electrochemically
189 equivalent “layers” as shown in the Figure 1a.

190

191 **b) High-frequency intercept R_s (conventional liquid electrolytes)**

192 At high frequencies in MHz range some capacitance elements such as C_ϵ and $c_{\epsilon,i}$ (Figure 1b)
193 are already “open” – *i.e.* the associated displacement current practically ceases, thus the
194 corresponding coupled resistances of electrolyte in the separator ($R_b(sep.)$) and in pores of
195 cathode composite ($r_{pore,i}$) appear as a pure resistances and it can be considered as a main
196 contribution for R_s . Most of the other capacitance elements have much larger magnitudes
197 (higher time constants and can be neglected).

198 At the high-frequency equivalent circuit there are no elements related to Li-anode – thus
199 according to the present interpretation Li-anode does not contribute to R_s . This is strictly valid
200 for “smooth” non-cycled Li-anode (as for example anode in initial state after cell assembly).
201 During cycling surface morphology of metal Li gradually becomes more and more
202 “roughened” and eventually even disintegrated during repeatable Li stripping and
203 plating.^{43,47,48} In that way a sort of porous-like Li-anode is formed that can bring contribution
204 to R_s .

205 Thus we find that the contribution of cathode to R_s is composed of two parts: a) Contribution
206 of porous composite that amounts in the equivalent resistance for the parallel combination of
207 $R_{cath.}$ and R_{pore} ; b) Contribution of interface at the surface of current collector that amounts
208 in the equivalent resistance for the parallel combination of r_0 and $r_{pore,0}$. Therefore, in
209 principle both pairs ($R_{cath.}||R_{pore}$ and $r_0||r_{pore,0}$) do contribute partially to R_s . However, in
210 real cells the second pair can be generally neglected, as the resistance of element $r_{pore,0}$ is

211 very small. In practice, for a cathode to give rise of a significant contribution to R_s its
212 electronic ($R_{\text{cath.}}$) and ionic (R_{pore}) resistances would have to be largely increased at the
213 same time. For Li-S cells with conventional liquid electrolytes this is rather unlikely to be the
214 case during individual discharge/charge – for instance during discharge the precipitation of
215 solid Li_2S can reduce electrode porosity and thereby increase R_{pore} , but in the initial part of
216 the same discharge insulating elemental sulfur is consumed which might even decrease the
217 $R_{\text{cath.}}$. On the contrary, during long term cycling $R_{\text{cath.}}$ might gradually increase due to: i)
218 loosen electronic connectivity of the composite (reduced mechanical integrity due to local
219 volume changes associated with repeatable dissolution/precipitation of solid S_8 and Li_2S
220 phases); ii) possible (chemical/electrochemical) formation of electronically non-conductive
221 films at the surface of conductive matrix and/or carbon black particles; and iii) decreased
222 conductivity of electrolyte in the pores. These effects can result in a slow gradual increase of
223 R_s during cycling. Thus for Li-S cells with conventional liquid electrolytes the regularly
224 observed peculiar periodic variation of R_s during the course of individual cycle is most
225 probably not related to concurrent increase of the $R_{\text{cath.}}||R_{\text{pore}}$ pair but rather to the increase
226 of $R_b(\text{sep.})$ alone. Although R_{pore} increases in accordance with the increase of specific bulk
227 resistance of electrolyte (ρ_b) it does not contribute to the R_s as it is “shielded” by low
228 resistance $R_{\text{cath.}}$.

229 Alternatively, during cycling of a Li-S cell the inclusion/incorporation of the non-conductive
230 products of side reactions (for instance Li_2S) within the native anode passive film at the
231 surface of Li metal anode ($R_{\text{film}}(\text{Li})$) can produce additional contributions to R_s .

232 In the measured R_s there are also included other (minor) Ohmic resistances due to different
233 external (resistance of connection wires – leads, cell terminals) and internal cell electronic
234 contributions (contacts between internal current leads and the two current collectors,
235 electronic resistance of Li-anode). All of these contributions are generally small compared to

236 the $R_b(sep.)$, R_{pore} and r_0 and more importantly do not vary during the cell operation – thus
237 do not contribute to the observed variation of R_s .

238

239 **c) High-frequency intercept R_s (GPE-PIL electrolyte)**

240 For cells that include polymeric or gel type of electrolyte there are additional issues related to
241 viscoelastic properties of such medium exposed to the influence of mechanical stresses that
242 are induced when growth of a new solid phase is taking place in the volume of the medium.
243 For example while discharging the solvent-free Li-S cell a newly formed solid Li_2S phase at
244 the surface of carbon matrix pushes away the adjacent volume of the GPE-PIL thus imposing
245 stresses shear in the electrode. Opposite effect can be expected at the end of charge when
246 solid S_8 is formed. During cycling repeatable formation and decomposition of the two solid
247 phases takes place and consequently binder in the composite is subjected to local variations of
248 stress that can result in severely loosen cathode (electronic) connectivity. Accordingly, the
249 $R_{cath.}$ greatly increases. Moreover, if at the same time the conductivity of electrolyte in the
250 cathode pores is reduced consequently the contribution of $R_{cath.}||R_{pore}$ pair to R_s becomes
251 large. Thus we see that in case of the cells where cathode is impregnated with (solvent-free)
252 GPE-PIL the R_s is not dependent solely upon the resistance of electrolyte layer between
253 cathode and anode, but cathode contribution can become important.

254

255 **3.2 Electrochemical performance of the Li-S batteries that include GPE-PIL** 256 **components**

257 The schematic view of the cross-section of the three battery configurations used in the present
258 study are shown in the Figure 2.

259 **a) Solvent-free configuration**

260 Results of galvanostatic cycling at C/40 rate obtained at 55 °C with the solvent-free
261 configuration show two characteristic plateaus in the first discharge (Figure 3a). That
262 indicates the mechanism of sulfur conversion into polysulfides at the high voltage plateau and
263 precipitation of Li₂S in the low voltage plateau.⁸ The specific discharge capacity in the first
264 cycle exceeds 1400 mAh g⁻¹. Similar to the first discharge, the first charge shows distinctive
265 voltage profiles as observed in the conventional Li-S batteries with ether-based electrolytes.
266 The total polarization in the first cycle (voltage hysteresis at approximately half of the
267 obtained discharge/charge capacity ~390 mV) is slightly higher as compared to the
268 conventional Li-S battery cycled at room temperature (~330 mV).⁴¹ The polarization issues
269 become more pronounced in the subsequent cycles where a severe and continuous increase of
270 the galvanostatic hysteresis can be seen (for instance ~900 mV in the fifth cycle, Figure 3a).
271 The noticeable increase in the internal resistance is reflected by significant capacity fading,
272 for *e.g.* only half of the initial capacity was achieved after the first 10 cycles with an average
273 coulombic efficiency of 98.1% (Figure 3b). In the higher cycles, the increase of polarization
274 can contribute to the corrosion of aluminum current collector caused by high potential during
275 charging. In order to understand correlation between the increase of the internal resistance of
276 the cell and consequent increase of the polarization, we performed comparative EIS
277 experiments. Prior to taking measurements, the battery was left for 3 h at 55 °C to thermally
278 equilibrate and stabilize impedance responses. We performed the following repeating
279 sequence: partial discharge (charge) at C/40 for 2.5 h, open-circuit voltage relaxation for 25
280 minutes, and EIS measurement (1 MHz – 10 mHz). The first two cycles obtained with a
281 repeating sequences of intermittent galvanostatic cycling, voltage relaxations and EIS are
282 shown in Figure 3c. Electrochemical behavior in the first cycle was similar to the one
283 obtained with the continuous galvanostatic cycling, while a prominent decrease of capacity
284 was observed in the second cycle. From the impedance spectra shown in Figure S4, the values

285 of resistive intercept R_s have been collected and the extracted values for both cycles are
286 presented in Figure 3d.

287 Figure 3d shows that during the first discharge there was only mild variation of R_s . Almost
288 monotonous increase from 16.0Ω up to 21.6Ω was observed. This is essentially different
289 from the observation found in the conventional Li-S cells, where a very pronounced maxima
290 of R_s is correlated with the increase in the viscosity of electrolyte due to increased
291 concentration of medium chain polysulfides.⁴⁹ Measurements during the first charge show
292 such an increase (after $\sim 300 \text{ mAh g}^{-1}$), but in contrast to conventional Li-S cells R_s did not
293 decrease at the end of discharge but rather remained constant ($\sim 31 \Omega$). The value of R_s
294 practically doubled during the first cycle. In the initial part of the second discharge, an abrupt
295 increase of R_s was observed that increased even further, to finally reach $\sim 90 \Omega$. At the end of
296 the second charge, only minor decrease of R_s was observed. As already discussed above we
297 the observed pronounced increase of R_s to such large values is connected to coupled effects of
298 reduced GPE-PIL conductivity (caused by dissolution of polysulfides) that increases both
299 membrane resistance ($R_b(\text{membr.})$) as well as resistance of GPE-PIL in pores (R_{pore}), and
300 reduced cathode electronic connectivity (increased $R_{\text{cath.}}$).

301 We propose that the thick GPE-PIL layer in solvent-free configuration denotes a larger
302 volume of a medium (larger diffusion distance) in which (additionally) the rate of diffusion of
303 polysulfides is reduced in comparison to conventional liquid electrolytes. Thus, the expected
304 periodical variation of R_s during discharge and charge was not seen (Figure 3c-d), instead an
305 increase is observed. During the discharge, for example, the reduction of R_s does not take
306 place since the cathode cannot “pump back” all the polysulfides that have diffused a certain
307 critical distance into the GPE-PIL phase away from the surface of the cathode conductive
308 matrix. During the experiment with partial discharge (charge) steps combined with open-
309 circuit relaxation and EIS measurements, the increase in the polarization was even more

310 pronounced in comparison to continuous galvanostatic cycling. Faster increase of polarization
311 can be correlated to additional time available for the diffusion of polysulfides (due to
312 relaxation periods). Specifically, during the relaxation periods, the cathode does not collect or
313 “pump back” any of the polysulfides from the GPE-PIL (even those that are normally in the
314 vicinity of the cathode during continuous cycling). Thus more of the polysulfides travel deep
315 into the interiors of GPE-PIL, where they become inaccessible for electrochemical
316 transformation and may eventually reach the metallic Li-anode for chemical reduction to take
317 place.

318 **XPS analysis**

319 In order to better investigate the precise mechanisms leading to the polarization and
320 impedance increase in the batteries, we carefully analyzed the internal parts of the cells with
321 XPS. Precisely, two analyzed samples are depicted in Figure S3, *i.e.* (i) the lithium negative
322 electrode surface facing the GPE-PIL electrolyte, and (ii) the GPE-PIL electrolyte surface
323 facing the lithium electrode (the sulfur composite cathode impregnated by the GPE-PIL
324 cannot be separated from the GPE-PIL membrane).

325 XPS results obtained for the Li-anode surface are shown in Figure 4. After the first discharge
326 (Figure 4a), the surface of metallic lithium is covered by several recognizable species. Due to
327 spin-orbit coupling, S $2p$ peaks are split into two components (S $2p_{3/2}$ and S $2p_{1/2}$) with
328 ~ 1.2 eV binding energy difference and a 2/1 intensity ratio. The main peak (S $2p_{3/2}$ at around
329 169.4 eV) is assigned to TFSI⁻ anion.⁵⁰ Another weak component is observed at slightly lower
330 binding energy (~ 167.5 eV). This latter component was already observed by XPS in Li-S
331 batteries and was attributed to S(IV) degradation species of the salt, which could be a sulfite
332 species, such as LiSO₂CF₃ or Li₂(F₃C-SO₂-N-SO₂),⁴² or even Li₂SO₃ already proposed by
333 Aurbach et. al.²⁴ The most interesting signals of the spectrum are the two components
334 observed at low binding energy, *i.e.* ~ 162 and ~ 163.6 eV (blue and red, respectively). The

335 components are attributed to the terminal and bridging sulfur atoms of Li_2S_n polysulfides,
336 respectively. The presence of polysulfides at the surface of the metallic Li-anode proves the
337 diffusion and/or migration of these species from the sulfur composite cathode towards the Li-
338 anode through the GPE-PIL electrolyte. Their relative intensity ratio shows that short chain
339 polysulfides are observed at the surface (mainly Li_2S_2). However, the intensity of these two
340 peaks is quite weak and dramatically much lower than in the case of a liquid electrolyte.⁴²
341 Moreover, no Li_2S component can be observed after the first discharge. Therefore, it can be
342 concluded that the GPE-PIL electrolyte in solvent-free configuration retards the polysulfide
343 diffusion from the sulfur composite cathode to the Li-anode. Substantial modifications are
344 observed after several cycles. Figure 4b shows the S 2*p* spectrum of the Li-anode after the 5th
345 discharge. In this case, the amount of polysulfides is increased (mainly Li_2S_2), and the largest
346 component of the spectrum (~160.5 eV, pink) is now assigned to Li_2S . Therefore, a
347 significant diffusion of polysulfides have occurred during several cycles, leading to a massive
348 reduction of these species into Li_2S at the surface of metallic Li-anode.

349 This study was complemented by XPS analysis of the GPE-PIL surface facing the Li-anode,
350 as shown in Figure 5. The XPS S 2*p* spectrum of the pristine GPE-PIL membrane (Figure 5a)
351 shows a unique peak attributed to the TFSI^- anion, as expected. After the first discharge
352 (Figure 5b) the spectrum slightly changes, with the appearance of the aforementioned sulfite
353 degradation compound of the salt, as well as a very weak signature of the polysulfide species.
354 This is in good agreement with the observation of a small amount of polysulfides at the
355 surface of the Li-anode at the end of the first discharge, indicating the passage of polysulfides
356 (to a low extent) across the gel polymer electrolyte.

357 After the first charge (Figure 5c) the spectrum is not much modified with respect to the first
358 discharge. However, after the 5th discharge (Figure 5d) the S 2*p* spectrum is significantly
359 changed. The amount of polysulfides is multiplied by 20 with respect to the first discharge.

360 This is in good agreement with the observation of a great amount of Li_2S and short chain
361 polysulfides at the surface of the Li-anode and shows that a great number of polysulfides
362 reaches the opposite surface of the gel polymer electrolyte after several cycles. Note that the
363 bridging-to-terminal sulfur intensity ratio is inverted with respect to the Li-anode surface.
364 This means that longer chain polysulfides are observed at the gel polymer electrolyte surface
365 facing the Li-anode. This is in good agreement with the reduction mechanism of polysulfides
366 (and thus the decrease of their chain length) at the surface of the Li-anode, as expected.
367 All these XPS observations are consistent with the EIS measurements (variation of R_s) as
368 discussed above.

369 Although at the present stage of the research of the solvent-free configuration we cannot
370 directly claim which of the contributions to the cell's internal resistance is dominantly
371 responsible for the observed rapid increase of polarization during cycling, the present data and
372 analysis offer several interesting observations and findings:

- 373 a) The initial cell polarization is slightly larger compared to the case of Li-S battery with
374 conventional liquid electrolyte (at 25 °C), the difference (~60 mV) being of the
375 magnitude that could be explained by the contribution of the resistance associated with
376 Li^+ ion conduction process in the GPE-PIL components.
- 377 b) Pronounced increase of R_s during cycling is indicating that both ionic (R_{pore}) and
378 electronic (R_{cath}) resistances of the cathode have increased, suggesting that internal
379 stresses in the composite might have loosen cathode (electronic) connectivity.
380 Alternatively, formation of Li_2S on Li-anode surface could bring about (or partly
381 contribute) to the observed severe increase of R_s .
- 382 c) The GPE-PIL layer does not prevent diffusion of polysulfides but merely hinders it (to
383 diffuse over ~400 μm length during intermittent cycling we estimate that the time
384 needed is ~70 h).

385

386 **b) Hybrid configuration**

387 In order to minimize the “buffer effect” of the GPE-PIL electrolyte where polysulfides can be
388 trapped and thus becoming unavailable for the main electrochemical transformation, different
389 approach has been studied. One of the possibilities is embedding of the agglomerates of C-S
390 composite in a gel polymer electrolyte without using any additional binder or additional
391 carbon additive. With this approach, 35–60 wt. % of sulfur content has been achieved within
392 the C-S composite. Composites with 10 and 25 wt. % of GPE-PIL showed polysulfides
393 shuttling in early cycles while cycling with 50 wt. % of GPE-PIL exhibits very stable cycling,
394 as shown in Figure 6. To evaluate the performance of composites containing GPE-PIL, a
395 battery in the conventional configuration using PVdF as a binder within the composite
396 electrode has been cycled for comparison. Figure 6 compares three cells, two with gel
397 polymer electrolyte based on PIL using different liquid electrolyte and the third one with
398 PVdF binder. In the formation cycles, about a 20% lower capacity was obtained in the case of
399 PVdF binder using liquid electrolyte (1M LiTFSI TEGDME:Diox), which could be correlated
400 to the hydrophobic nature of PVdF whereby the region of the electrode composite covered
401 with the PVdF are substantially less accessible to Li^+ ions from the electrolyte phase.
402 Surprisingly, batteries with GPE-PIL binder using the same liquid electrolyte (1M LiTFSI
403 TEGDME:Diox) show very similar coulombic efficiency (in average 94%), while the battery
404 with 1M LiTFSI DME:Diox electrolyte shows much higher coulombic efficiency (in average
405 99.2%). Moreover, working with a low amount of electrolyte has an impact on the cycle life.
406 As can be seen in Figure 6, the capacity of the cell with the PVdF binder exhibited increasing
407 degradation (evident after $\sim 50^{\text{th}}$ cycle) while in contrast the cell with the gel polymer
408 electrolyte showed moderate, practically constant degradation of the capacity until 100 cycles.
409 This observation indicates that the present novel approach in which the binder (PVdF) was

410 replaced with GPE-PIL-based gel demonstrates beneficial properties with enhanced stability
411 of the Li-S electrochemical system.

412 The results are preliminary and after optimization one can expect composites with similar
413 behavior containing a much lower quantity of GPE-PIL. In contrast, this work points out the
414 requirement for optimal thickness, where GPE-PIL presumably serves as a barrier for keeping
415 polysulfides close to the surface of the carbon host matrix. By the present interpretation the
416 role of the “wetted” GPE-PIL is then to prevent the fast diffusion of polysulfides out from the
417 cathode and enable their effective conversion in the discharge or the charge process.
418 However, such pre-treatment allows using a lower amount of liquid electrolyte (GPE-PIL is,
419 in fact, a gel polymer electrolyte). Only one layer of Celgard 2400 separator was used in the
420 battery assembly. Taking the calculated porosity 63 vol. % of porosity of the composite
421 cathode, the amount of electrolyte within the cathode and the separator is between 2–3 μL per
422 1 mg of sulfur. This amount of electrolyte used in our experiment approaches the
423 requirements of achieving a high energy density of the Li-S battery system^{4,13}. In this work,
424 we use only one potential gel polymer electrolyte; however, some other types of gel polymer
425 electrolytes based on the polymer ionic liquids are available for any potential improvements.
426 The morphological changes in the cross-section of the electrode after 100 cycles were
427 checked by using SEM. Figure 7a shows the morphology of the composite cathode containing
428 $\text{C}_{\text{Ecp600JD}}\text{-S}$ composite covered with 50 wt. % of the GPE-PIL before cycling. The
429 morphological changes after 100 cycles are minor, proving the good stability of the electrodes
430 comprising GPE-PIL-based gel type coating (Figure 7b).

431 Additional information about the cell performance using different components can be
432 obtained by a direct comparison of the galvanostatic curves in different cycles. Figure 8
433 shows the 1st, 10th, 50th and 100th cycles for batteries with gel polymer electrolyte in the
434 composite cathode in combination with two different electrolytes and for the battery with

435 PVdF binder. The voltage value of the high voltage plateau in the cell with 1M LiTFSI
436 TEGDME:Diox electrolyte (Figure 8a) is approximately 100 mV higher compared to the cell
437 with 1M LiTFSI DME:Diox electrolyte (Figure 8b). The low voltage plateau is relatively flat
438 in both cases, not showing any increase in the polarization during cycling. The discharge
439 curves obtained from the battery with PVdF binder show a pronounced increase of
440 polarization during cycling, particularly at the transition from the high to low voltage plateau,
441 which was observed as a distinctive saddle-like appearing local minima in a voltage profile.
442 The related increase in polarization is due to oversaturation of the electrolyte with
443 polysulfides, and this gradually increases upon cycling. The reasons for the saturation of the
444 electrolyte with polysulfides can be manifold. Among all the possibilities, the most probable
445 is the saturation of the electrolyte with polysulfides due to continuous polysulfide diffusion
446 out from the composite cathode; additionally, we can expect some electrolyte degradation on
447 the fresh surface of Li-anode formed during the stripping and plating of lithium. In addition to
448 increased polarization, the battery with PVdF binder suffered distinct polysulfide shuttle
449 (Figure 8c).

450 Kinetic issues shown in the solvent-free configuration compromise the power capability of the
451 battery with the GPE-PIL. However, it is expected that the quantity of the GPE-PIL as well as
452 the quantity of added liquid electrolyte (“wetting condition”) in the cell plays very important
453 role in the Li-S battery kinetics. Figure 9a shows rate capability of the battery with 50 wt. %
454 of GPE-PIL in the composite cathode at different current densities corresponding to $C/20$ to
455 $1C$ (1.67 mA mg^{-1}) and back to $C/20$. The capacity drop between $C/20$ and $C/2$ corresponds
456 to one third of the initial capacity value, and it is recovered at the slower C -rates. Severe
457 capacity drop occurs as the C -rate is increased up to $1C$, as the capacity of the lower plateau
458 cannot be utilized anymore in the voltage window used ($1.5\text{--}3 \text{ V}$). Figure 9b shows the
459 galvanostatic curves of the rate capability, with the formation cycle at $C/50$ and going from

460 C/20 to 1C and back to C/20. Two well defined plateaus are expressed till C/5 rate. At C/2 an
461 increase in polarization is observed, and at 1C a disappearance of the low voltage plateaus.
462 Going back to lower C-rates, the polarization decrease and the low voltage plateau is well
463 defined.

464

465 **4. Conclusions**

466 Solvent-free configuration of the Li-S battery where the GPE-PIL serves as an electrolyte and
467 as separator offers a system in which the solubility of polysulfides occurs in the ionic liquid
468 nested in the polymer matrix. This battery delivers high initial capacity when operated at
469 elevated temperatures (at 55 °C), and is accompanied with an effect of delayed diffusion of
470 polysulfides through the thick GPE-PIL layer to reach Li-anode. XPS results show that the
471 amount of sulfur species on the lithium surface is very low after the first discharge, while Li₂S
472 and polysulfides can be detected on the lithium surface after several cycles. This was
473 confirmed with EIS, where we observed that the series resistance (R_s) and thus the related
474 bulk resistivity of the GPE-PIL did not show usual periodic increase/decrease behavior during
475 cycling but rather delayed response where the initial mild increase gradually developed in
476 severe rise during 2nd cycle and further remained at that high value. Both these techniques are
477 indicating that larger amounts of polysulfides are inevitably lost in the volume of GPE-PIL of
478 the solvent-free Li-S battery. We cannot conclude if this is the only reason for the increase of
479 polarization at the present stage of the research. More systematic work where increase of
480 interphase resistance on the lithium surface and disintegration of the cathode composite need
481 to be done in the future to understand function of PIL within the Li-S batteries. Furthermore,
482 impact of polysulfide dissolution into GPE-PIL phase will be studied by performing
483 measurements on symmetrical cells and Li-S battery cells.

484 In the hybrid cell configuration, we prepared the cathodes by embedding the agglomerates of
485 the sulfur/carbon composite in the GPE-PIL electrolyte “coating” without using any
486 additional binder or carbon additive. The long-term cycling stability of electrodes containing
487 the GPE-PIL is improved compared to electrodes using PVdF as a binder. The GPE-PIL layer
488 on the surface of the sulfur/carbon agglomerates in combination with liquid electrolyte
489 probably serves as a buffer where polysulfides are dissolved but, due to slow diffusion in the
490 gel type electrolyte, they are presumably retained within the vicinity of the composite
491 cathode. The hybrid cell configuration offers a system with improved electrochemical
492 stability, where the key role of the GPE-PIL “coating” at the present stage is not understood
493 enough, thus the future efforts will be directed in the study of (chemical, morphological, and
494 transport) properties of the layer at the surface of C/S particles.

495

496

497 **Acknowledgements**

498 This research has received funding from the Slovenian Research Agency (J2-5469) and the
499 European Union Seventh Framework Programme under grant agreement No. 314515
500 (EUROLIS).

501 **Figure captions:**

502

503 **Figure 1:** a) Schematic representation of a Li-S battery cell comprising a Li metal anode, a
504 separator soaked with liquid electrolyte and a porous (conductive matrix-sulfur) composite
505 cathode. b) Proposed Equivalent Circuit of a Li-S battery that comprises anode, separator, and
506 a porous (conductive matrix-sulfur) composite cathode. The contribution(s) of the porous
507 cathode can be essentially presented by a modified type of the transmission line model that
508 was used for the interpretation of electro-chemical properties of multi-particle Li-ion insertion
509 cathodes.^{45,46} c) Proposed simple High-Frequency (~MHz) Equivalent Circuit. For the
510 meaning and role of the main resistive and capacitive elements see the text.

511

512 **Figure 2:** The schematic view of the cross-section of the a) the solvent-free, b) hybrid and c)
513 conventional configuration.

514

515 **Figure 3:** Tested battery configuration: C/S cathode impregnated with GPE-PIL pressed to a
516 GPE-PIL membrane (thickness of 390 μm) in direct contact with metallic lithium: a)
517 galvanostatic C/40 curves of the 1st, 5th, 15th and 30th cycle measured at 55 °C b) cycling
518 stability c) two cycles of galvanostatic cycling at C/40 rate with relaxation periods after
519 $\Delta x = 0.06$ and d) values of corresponding bulk conductivity R_s extracted from impedance
520 spectra measured at the end of each relaxation period.

521

522 **Figure 4:** XPS S 2p spectra of the lithium electrode obtained after a) 1st discharge and b) 5th
523 discharge in solvent-free configurations.

524

525 **Figure 5:** XPS S 2p spectra of the GPE-PIL surface facing the Li-anode in solvent-free
526 configurations: a) pristine, b) after 1st discharge, c) after 1st charge and d) after 5th discharge.

527

528 **Figure 6:** Discharge capacity (left y-axis) and coulombic efficiency (right y-axis) for Li-S
529 batteries with GPE-PIL-C_{Ecp600JD}-S composite using 1M LiTFSI in TEGDME:Diox
530 electrolyte, GPE-PIL-C_{Ecp600JD}-S composite using 1M LiTFSI in DME:Diox electrolyte and
531 PVdF-C_{Ecp600JD}-S composite using 1M LiTFSI in TEGDME:Diox. Batteries were cycled with
532 a current density corresponding to C/20 rate between 1.5 and 3 V at RT (25 °C).

533

534 **Figure 7:** SEM micrographs of the GPE-PIL-C_{Ecp600JD}-S: a) before cycling and b) after 100
535 cycles.

536

537 **Figure 8:** Galvanostatic curves in the 1st, 10th, 50th and 100th cycle measured using C/20 rate
538 at RT (25 °C) for the cell configurations: a) GPE-PIL-C_{Ecp600JD}-S composite with 1M LiTFSI
539 in TEGDME:Diox using Celgard 2400 separator; b) GPE-PIL-C_{Ecp600JD}-S composite with 1M
540 LiTFSI in DME:Diox using Celgard 2400 separator and c) PVdF-C_{Ecp600JD}-S composite with
541 1M LiTFSI in TEGDME:Diox using Celgard 2400 separator.

542

543 **Figure 9:** a) Rate capability of Li-S battery using GPE-PIL-C_{Ecp600JD}-S composite, 1M
544 LiTFSI in TEGDME:Diox and Celgard 2400 separator at various discharge and charge rates
545 from C/20 to 1C and back to C/20 obtained at RT (25°C) and b) corresponding galvanostatic
546 curves (solid curves corresponds to applied current densities during increase of the C-rate and
547 dashed curves correspond to decrease of the C-rate).

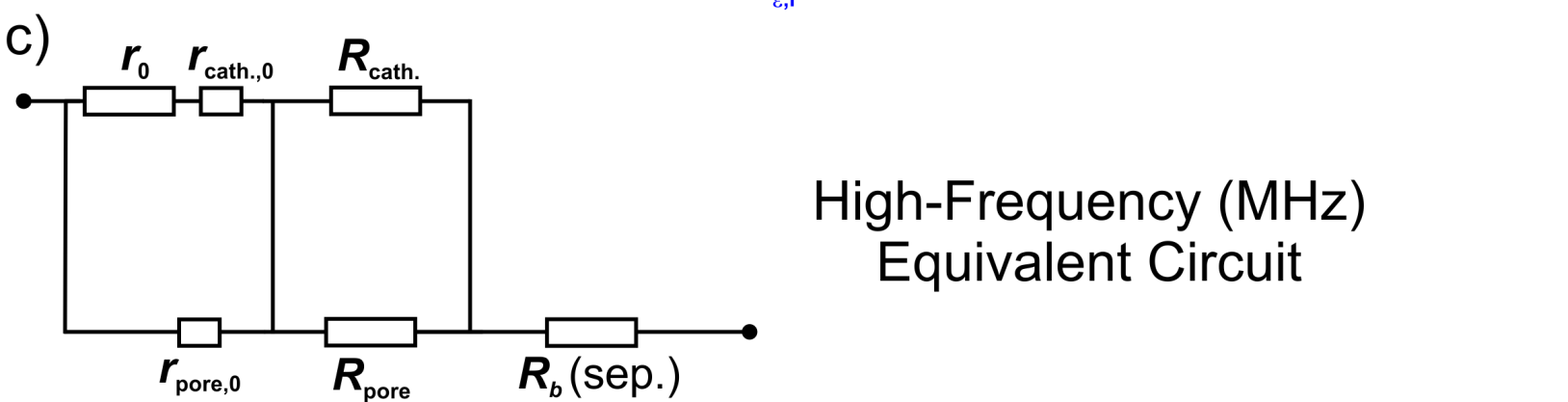
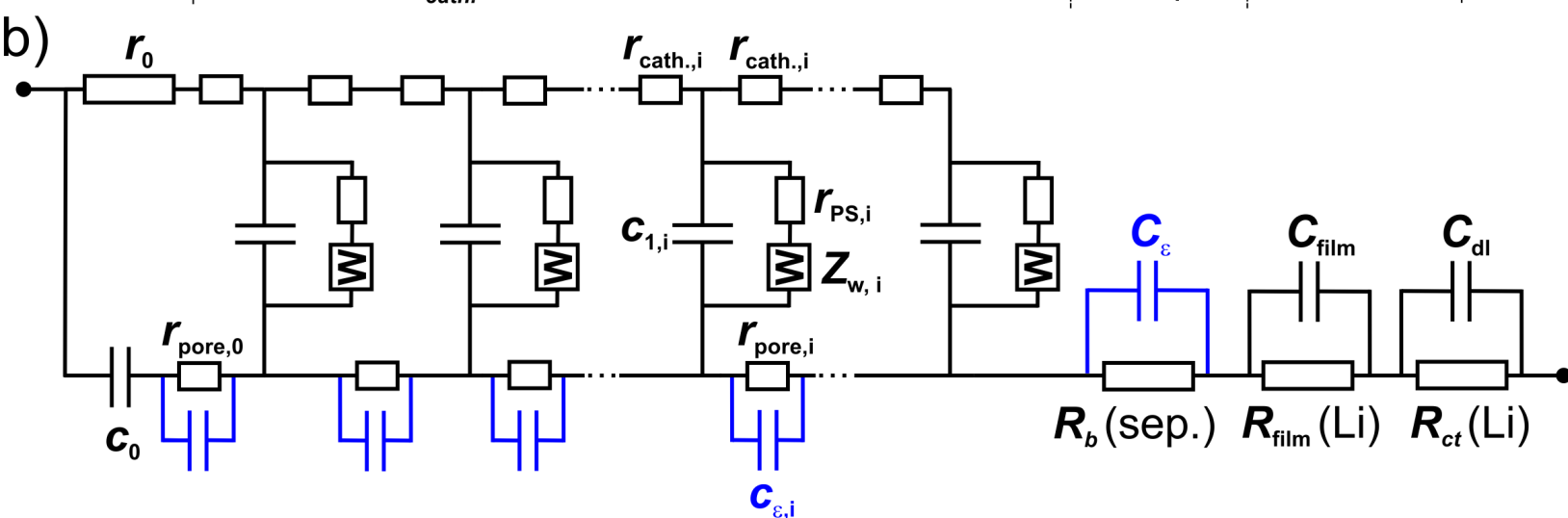
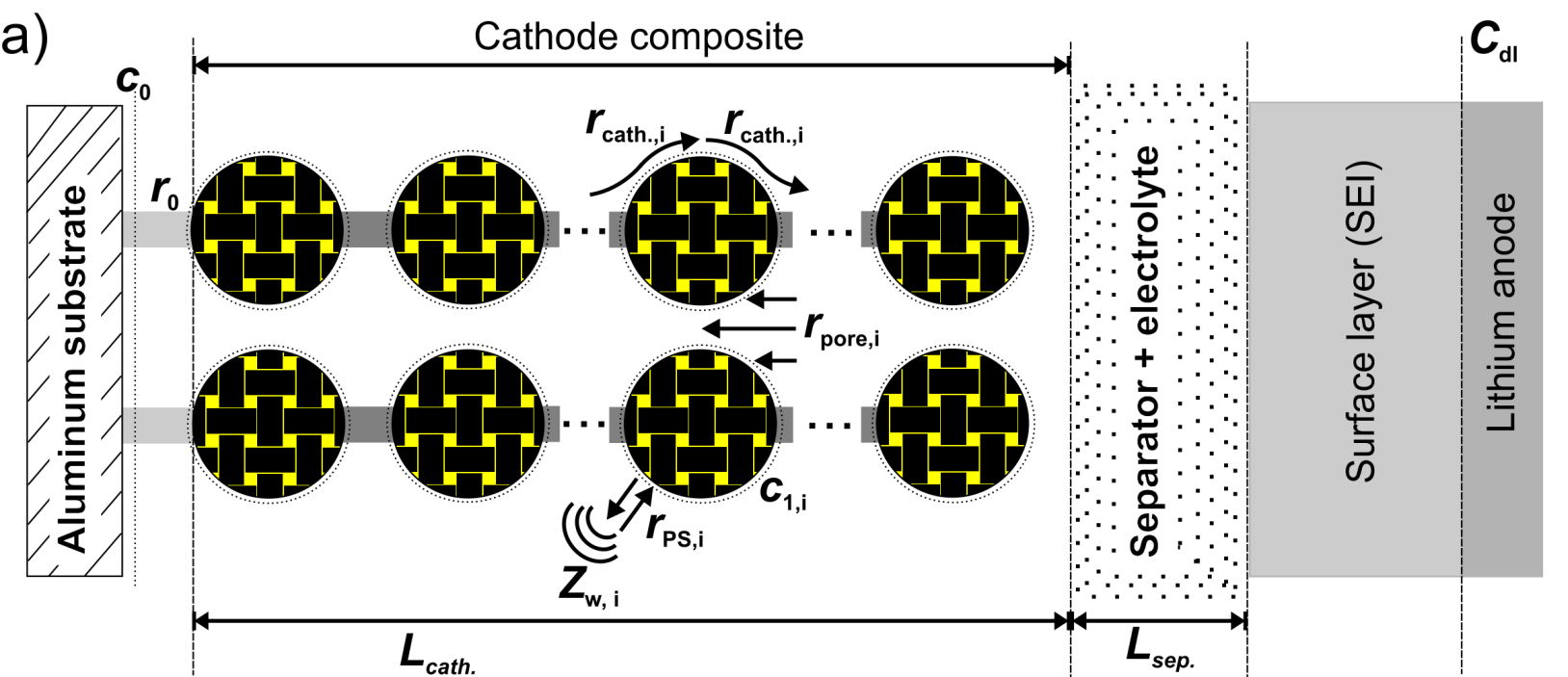
548

549 **References**

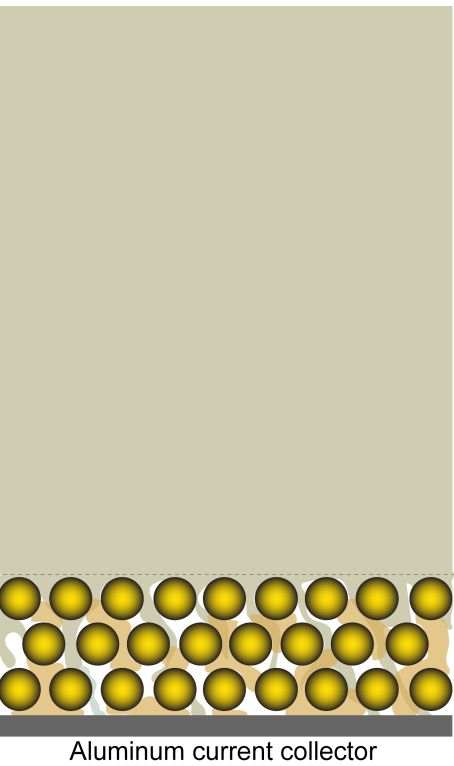
- 550 1. P. G. Bruce, S. A. Freunberger, L. J. Hardwick, and J.-M. Tarascon, *Nat. Mater.*, **11**, 19
551 (2011).
- 552 2. B. Dunn, H. Kamath, and J.-M. Tarascon, *Science*, **334**, 928 (2011).
- 553 3. A. Rosenman, E. Markevich, G. Salitra, D. Aurbach, A. Garsuch, and F. F. Chesneau, *Adv.*
554 *Energy Mater.*, **5**, 1500212 (2015).
- 555 4. M. Hagen, D. Hanselmann, K. Ahlbrecht, R. Maça, D. Gerber, and J. Tübke, *Adv. Energy*
556 *Mater.*, **5**, 1401986 (2015).
- 557 5. R. D. Rauh, F. S. Shuker, J. M. Marston, and S. B. Brummer, *J. Inorg. Nucl. Chem.*, **39**,
558 1761 (1977).
- 559 6. R. D. Rauh, K. M. Abraham, G. F. Pearson, J. K. Surprenant, and S. B. Brummer, *J.*
560 *Electrochem. Soc.*, **126**, 523 (1979).
- 561 7. Y. V. Mikhaylik and J. R. Akridge, *J. Electrochem. Soc.*, **151**, A1969 (2004).
- 562 8. R. Dominko, M. U. M. Patel, V. Lapornik, A. Vizintin, M. Koželj, N. N. Tušar, I. Arčon,
563 L. Stievano, and G. Aquilanti, *J. Phys. Chem. C*, **119**, 19001 (2015).
- 564 9. X. Ji, K. T. Lee, and L. F. Nazar, *Nat. Mater.*, **8**, 500 (2009).
- 565 10. Y.-X. X. Yin, S. Xin, Y.-G. G. Guo, and L.-J. J. Wan, *Angew. Chem. Int. Ed.*, **52**, 13186
566 (2013).
- 567 11. S. Evers and L. F. Nazar, *Acc. Chem. Res.*, **46**, 1135 (2013).
- 568 12. R. Demir-Cakan, M. Morcrette, F. Nouar, C. Davoisne, T. Devic, D. Gonbeau, R.
569 Dominko, C. Serre, G. Férey, and J. M. Tarascon, *J. Am. Chem. Soc.*, **133**, 16154 (2011).
- 570 13. M. A. Pope and I. A. Aksay, *Adv. Energy Mater.*, **5**, 1500124 (2015).
- 571 14. S. Evers, T. Yim, and L. F. Nazar, *J. Phys. Chem. C*, **116**, 19653 (2012).
- 572 15. Y. Yang, G. Zheng, and Y. Cui, *Chem. Soc. Rev.*, **42**, 3018 (2013).
- 573 16. S. Urbonaite, T. Poux, and P. Novák, *Adv. Energy Mater.*, **5**, 1500118 (2015).
- 574 17. J. Wang, Z. Yao, C. W. Monroe, J. Yang, and Y. Nuli, *Adv. Funct. Mater.*, **23**, 1194
575 (2013).
- 576 18. Y.-S. Su and A. Manthiram, *Chem. Commun.*, **48**, 8817 (2012).
- 577 19. A. Vizintin, M. U. M. Patel, B. Genorio, and R. Dominko, *ChemElectroChem*, **1**, 1040
578 (2014).
- 579 20. J.-Q. Huang, T.-Z. Zhuang, Q. Zhang, H.-J. Peng, C.-M. Chen, and F. Wei, *ACS Nano*, **9**,
580 3002 (2015).

- 581 21. J. Scheers, S. Fantini, and P. Johansson, *J. Power Sources*, **255**, 204 (2014).
- 582 22. S. S. Zhang, *J. Power Sources*, **231**, 153 (2013).
- 583 23. R. Demir-Cakan, M. Morcrette, Gangulibabu, A. Guéguen, R. Dedryvère, and J.-M.
584 Tarascon, *Energy Environ. Sci.*, **6**, 176 (2013).
- 585 24. D. Aurbach, E. Pollak, R. Elazari, G. Salitra, C. S. Kelley, and J. Affinito, *J. Electrochem.*
586 *Soc.*, **156**, A694 (2009).
- 587 25. Z. Lin, Z. Liu, W. Fu, N. J. Dudney, and C. Liang, *Adv. Funct. Mater.*, **23**, 1064 (2013).
- 588 26. S. Zhang, K. Ueno, K. Dokko, and M. Watanabe, *Adv. Energy Mater.*, **5**, 1500117 (2015).
- 589 27. M. Armand, *Solid State Ionics*, **69**, 309 (1994).
- 590 28. P. G. Bruce and C. A. Vincent, *J. Chem. Soc. Faraday Trans.*, **89**, 3187 (1993).
- 591 29. D. Baril, C. Michot, and M. Armand, *Solid State Ionics*, **94**, 35 (1997).
- 592 30. J. Jin, Z. Wen, X. Liang, Y. Cui, and X. Wu, *Solid State Ionics*, **225**, 604 (2012).
- 593 31. K. Jeddi, M. Ghaznavi, and P. Chen, *J. Mater. Chem. A*, **1**, 2769 (2013).
- 594 32. S. S. Zhang and D. T. Tran, *J. Mater. Chem. A*, **2**, 7383 (2014).
- 595 33. J. Wang, L. Liu, Z. Ling, J. Yang, C. Wan, and C. Jiang, *Electrochim. Acta*, **48**, 1861
596 (2003).
- 597 34. H. Schneider, A. Garsuch, A. Panchenko, O. Gronwald, N. Janssen, and P. Novák, *J.*
598 *Power Sources*, **205**, 420 (2012).
- 599 35. M. J. Lacey, F. Jeschull, K. Edström, and D. Brandell, *J. Phys. Chem. C*, **118**, 25890
600 (2014).
- 601 36. Z. W. Seh, Q. Zhang, W. Li, G. Zheng, H. Yao, and Y. Cui, *Chem. Sci.*, **4**, 3673 (2013).
- 602 37. S. Urbonaite and P. Novák, *J. Power Sources*, **249**, 497 (2014).
- 603 38. M. J. Lacey, F. Jeschull, K. Edström, and D. Brandell, *J. Power Sources*, **264**, 8 (2014).
- 604 39. Q. Wang, W. Wang, Y. Huang, F. Wang, H. Zhang, Z. Yu, A. Wang, and K. Yuan, *J.*
605 *Electrochem. Soc.*, **158**, A775 (2011).
- 606 40. G. B. Appetecchi, G.-T. Kim, M. Montanino, M. Carewska, R. Marcilla, D. Mecerreyes,
607 and I. De Meatza, *J. Power Sources*, **195**, 3668 (2010).
- 608 41. F. Schipper, A. Vizintin, J. Ren, R. Dominko, and T.-P. Fellingner, *ChemSusChem*, **8**, 3077
609 (2015).
- 610 42. A. Vizintin, M. Lozinšek, R. K. Chellappan, D. Foix, A. Krajnc, G. Mali, G. Drazic, B.
611 Genorio, R. Dedryvère, and R. Dominko, *Chem. Mater.*, **27**, 7070 (2015).




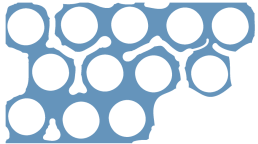

- 612 43. J.-J. Woo, V. A. Maroni, G. Liu, J. T. Vaughey, D. J. Gosztola, K. Amine, and Z. Zhang,
613 *J. Electrochem. Soc.*, **161**, A827 (2014).
- 614 44. G. Bieker, M. Winter, and P. Bieker, *Phys. Chem. Chem. Phys.*, **17**, 8670 (2015).
- 615 45. M. Gaberscek, J. Moskon, B. Erjavec, R. Dominko, and J. Jamnik, *Electrochem. Solid-
616 State Lett.*, **11**, A170 (2008).
- 617 46. J.-M. Atebamba, J. Moskon, S. Pejovnik, and M. Gaberscek, *J. Electrochem. Soc.*, **157**,
618 A1218 (2010).
- 619 47. C. M. López, J. T. Vaughey, and D. W. Dees, *J. Electrochem. Soc.*, **156**, A726 (2009).
- 620 48. C. M. López, J. T. Vaughey, and D. W. Dees, *J. Electrochem. Soc.*, **159**, A873 (2012).
- 621 49. S. Waluś, C. Barchasz, R. Bouchet, J.-C. Leprêtre, J.-F. Colin, J.-F. Martin, E. Elkaïm, C.
622 Baecht, and F. Alloin, *Adv. Energy Mater.*, **5**, 1500165 (2015).
- 623 50. R. Dedryvère, S. Leroy, H. Martinez, F. Blanchard, D. Lemordant, and D. Gonbeau, *J.
624 Phys. Chem. B*, **110**, 12986 (2006).
- 625



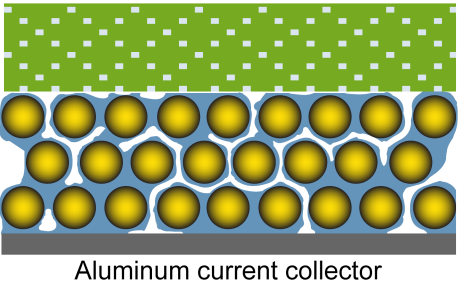
a) Solvent-free configuration



Legend:

-  Carbon/sulfur agglomerate
-  PVdF binder
-  GPE-PIL membrane
-  Soaked GPE-PIL binder with the electrolyte
-  Celgard 2400 separator: wetted with the electrolyte

b) Hybrid configuration



c) Conventional configuration

